Closed-loop Control of a Nonprehensile Manipulation System Inspired by the Pizza-Peel Mechanism

Alejandro Gutiérrez–Giles, Fabio Ruggiero, Vincenzo Lippiello and Bruno Siciliano

***Abstract*— A nonprehensile manipulation system consisting of a dexterous plate (e.g., a peel) which is intended to induce a rotating movement on a disk (e.g., a pizza) is studied. A dynamic model based on the Euler–Lagrange equations is first derived. Then, a controllability analysis of this model is carried out, which shows some intrinsic limitations of the proposed system. Later, a closed-loop control strategy is proposed to induce the desired rotating speed in the disk, while maintaining the position of both the disk and the plate as close to zero as possible. A stability analysis is performed to show the boundedness of all the states, the oscillatory response of all of them, and the maximum amplitude of these oscillations. A numerical simulation is employed to verify the proposed controller and the predicted behavior found in the stability analysis.**

I. Introduction

Nonprehensile manipulation consists in manipulating objects through a mechanical system (*e.g.,* a robot), but in contrast with the standard approach, the movement is induced without grasping the object to be manipulated. The main advantages of the nonprehensile manipulation are that it extends the workspace of the robot and the number of tasks it can perform. However, most of the times this tasks delivers the mechanical system to be underactuated (*i.e.,* fewer inputs than degrees of freedom). This implies that the controller design and the corresponding stability analysis usually are more complicated than in the standard manipulation case. Some early important achievements in this area are due to Lynch for the planar case [1]. A broad overview of the topic and state-of-the art are given in [2].

A complex nonprehensile manipulation task is commonly divided into more simple sub-tasks called *nonprehensile motion primitives*. Such primitives include rolling [3], [4], [5], sliding [6], object transportation [7], throwing [8], [9], and catching [10]. Most of these primitives are gathered in a recent paper [11], in the framework of the *RoDyMan* project[1].

The research leading to these results has been supported by the RoDyMan project, which has received funding from the European Research Council FP7 Ideas under Advanced Grant agreement number 320992. The authors are solely responsible for the content of this manuscript.

Alejandro Gutierrez–Giles is with CINVESTAV–IPN, Electrical Engineer Department, Mechatronics Section, Av. IPN 2508, San Pedro Zacatenco, 07300, Mexico City, Mexico, email: alejandro.giles@cinvestav.mx. Fabio Ruggiero, Vincenzo Lippiello and Bruno Siciliano are with CREATE Consortium and Prisma Lab. Department of Electrical Engineering and Information Technology, University of Naples Federico II, Via Claudio 21, 80125, Naples, Italy, emails: {fabio.ruggiero, vincenzo.lippiello, bruno.siciliano }@unina.it

[1]For more details visit: www.rodyman.eu

In this work, we are interested in a particular task concerning the sliding primitive. This task consists in inducing a rotating movement on a disk (pizza) by employing an actuated dexterous plate (peel), as shown in Figure 1. This system was inspired by the movements of the Italian pizza chefs and was initially proposed in [12]. Nevertheless, the problem of positioning objects by sliding was studied before in [13]. Later, in [14] the problem of positioning and orienting of a rigid body over a 2D plate was considered. Finally, a method for positioning and orienting a rigid body with a six-degrees-of-freedom rigid plate was proposed and successfully tested in [15]. From a practical point of view, nonprehensile manipulation through the sliding primitive is a very important control application in the industry, particularly in the so-called *part feeders*.

The problem of position and orientation control of a disk with a two-degrees-of-freedom manipulation system was addressed in [16]. In that work, the authors study the physical properties of the mechanical system to successfully drive the disk to an arbitrary position and orientation on the plate. They also show that the translation of the disk can be done without rotating the disk but not *vice versa*. However, in contrast with the linear positioning control scheme, the control strategy for the rotation part is mainly carried out in an open loop fashion, since no feedback of the disk rotation is employed in the control loop.

The main contribution of our work, in contrast with the mentioned above, is the design of a model based feedback control strategy. To the best of the authors' knowledge, this is the first attempt to propose such a strategy along with a closed-loop dynamic analysis that formally guarantees the good behavior of the system.

The rest of the manuscript is organized as follows: in Section II a dynamic model of the system based on the Euler–Lagrange formulation is derived. Furthermore, a controllability analysis is carried out to gain insight into the limitations of the model. In Section III a feedback control strategy is proposed to rotate the disk at a constant velocity while maintaining the remaining coordinates close to the origin. The corresponding closed-loop stability analysis is provided in the same section. A numerical simulation is given in Section IV to show the validity of the approach. Finally, some conclusions and directions for future work are given in Section V.

II. Mathematical Model

Let $\boldsymbol{o}_{\mathrm{w}}$–$\boldsymbol{x}_{\mathrm{w}}\boldsymbol{y}_{\mathrm{w}}\boldsymbol{z}_{\mathrm{w}}$ be the inertial frame, $\boldsymbol{o}_{\mathrm{h}}$–$\boldsymbol{x}_{\mathrm{h}}\boldsymbol{y}_{\mathrm{h}}\boldsymbol{z}_{\mathrm{h}}$ a frame attached to the plate and $\boldsymbol{o}_{\mathrm{p}}$–$\boldsymbol{x}_{\mathrm{p}}\boldsymbol{y}_{\mathrm{p}}\boldsymbol{z}_{\mathrm{p}}$ a frame attached

to the disk, as shown in Figure 1. The generalized coordinates for the plate, which is driven by a robotic manipulator, are given by $x_{\mathrm{h}} \in \mathbb{R}$ and $\theta \in \mathbb{R}$, where x_{h} is the first component of $\boldsymbol{o}_{\mathrm{h}}$ and θ is the rotation angle of the plate with respect to the inertial frame, defined by the basic rotation $\boldsymbol{R}_{\mathrm{h}} = \boldsymbol{R}_{\mathrm{x}}(\theta)$. The generalized coordinates for the disk are chosen as $x_{\mathrm{p}}, y_{\mathrm{p}}, \phi \in \mathbb{R}$, where x_{p} and y_{p} are the first two components[2] of $\boldsymbol{o}_{\mathrm{p}}^{\mathrm{h}}$, and ϕ is the angle of rotation of the disk with respect to the $\boldsymbol{z}_{\mathrm{p}}^{\mathrm{h}}$ axis, defined by the basic rotation matrix $\boldsymbol{R}_{\mathrm{p}}^{\mathrm{h}} = \boldsymbol{R}_z(\phi)$. The superscript denotes the frame in which the vector/matrix is expressed and it is omitted when referenced with respect to the world frame. Therefore, the configuration of the system is completely described by the vector

$$\boldsymbol{q} = \begin{bmatrix} x_{\mathrm{h}} & \theta & x_{\mathrm{p}} & y_{\mathrm{p}} & \phi \end{bmatrix}^{\mathrm{T}} . \tag{1}$$

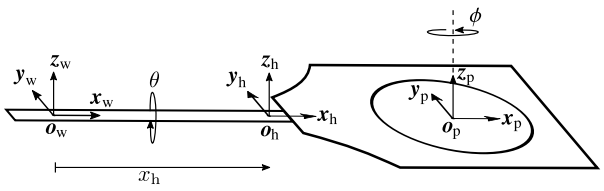

Fig. 1. Disk and plate system.

The position of the disk center of mass with respect to the world frame is given by

$$\boldsymbol{o}_{\mathrm{p}} = \boldsymbol{o}_{\mathrm{h}} + \boldsymbol{R}_{\mathrm{h}}\boldsymbol{o}_{\mathrm{p}}^{\mathrm{h}} = \begin{bmatrix} x_{\mathrm{h}} + x_{\mathrm{p}} & y_{\mathrm{p}}c_\theta & y_{\mathrm{p}}s_\theta \end{bmatrix}^{\mathrm{T}} , \tag{2}$$

where s_{x} and c_{x} are shorthand notations for $\sin(x)$ and $\cos(x)$, respectively. The orientation of the disk frame with respect to the inertial frame is described by the rotation matrix

$$\boldsymbol{R}_{\mathrm{p}} = \boldsymbol{R}_{\mathrm{h}}\boldsymbol{R}_{\mathrm{p}}^{\mathrm{h}} . \tag{3}$$

From this last matrix, one can obtain the disk angular velocity vector $\boldsymbol{\omega}_{\mathrm{p}}$ through the relation

$$\dot{\boldsymbol{R}}_{\mathrm{p}} = \boldsymbol{S}(\boldsymbol{\omega}_{\mathrm{p}})\boldsymbol{R}_{\mathrm{p}} , \tag{4}$$

where $\boldsymbol{S}(\cdot)$ is the standard skew-symmetric matrix operator, as explained for example in [17, p. 107].

The kinetic energy is given by

$$\mathcal{T}(\boldsymbol{q}, \dot{\boldsymbol{q}}) = \frac{1}{2}m_{\mathrm{h}}\dot{x}_{\mathrm{h}}^2 + \frac{1}{2}I_{\mathrm{hx}}\dot{\theta}^2 + \frac{1}{2}m_{\mathrm{p}}\dot{\boldsymbol{o}}_{\mathrm{p}}^{\mathrm{T}}\dot{\boldsymbol{o}}_{\mathrm{p}} + \frac{1}{2}\boldsymbol{\omega}_{\mathrm{p}}^{\mathrm{T}}\boldsymbol{R}_{\mathrm{p}}\boldsymbol{I}_{\mathrm{p}}\boldsymbol{R}_{\mathrm{p}}^{\mathrm{T}}\boldsymbol{\omega}_{\mathrm{p}} , \tag{5}$$

where m_{h} and m_{p} are the masses of the plate and the disk respectively, I_{hx} is the $(1,1)$ component of the inertia tensor of the plate, and $\boldsymbol{I}_{\mathrm{p}}$ is the inertia tensor of the disk, both with respect to their frame. The potential energy is

$$\mathcal{U}(\boldsymbol{q}) = m_{\mathrm{p}}g s_\theta y_{\mathrm{p}} , \tag{6}$$

where g is the gravity acceleration constant. To derive a dynamic model, consider the Euler–Lagrange equations of motion

$$\frac{\mathrm{d}}{\mathrm{d}t}\left(\frac{\partial \mathcal{L}}{\partial \dot{\boldsymbol{q}}}\right)^{\mathrm{T}} - \left(\frac{\partial \mathcal{L}}{\partial \boldsymbol{q}}\right)^{\mathrm{T}} = \boldsymbol{\xi} \tag{7}$$

with Lagrangian $\mathcal{L}(\boldsymbol{q}, \dot{\boldsymbol{q}}) = \mathcal{T}(\boldsymbol{q}, \dot{\boldsymbol{q}}) - \mathcal{U}(\boldsymbol{q})$. In this particular problem, the Coulomb friction terms play a crucial role for completing the task. These terms are defined as functions of the relative linear velocities of the disk $\dot{x}_{\mathrm{p}}$ and $\dot{y}_{\mathrm{p}}$ with respect to the plate referred to the plate frame, and are described by [16]

$$f_{\mathrm{x}} = -m_{\mathrm{p}}g\mu_{\mathrm{p}}\mathrm{sign}(\dot{x}_{\mathrm{p}}) \tag{8}$$

$$f_{\mathrm{y}} = -m_{\mathrm{p}}g\mu_{\mathrm{p}}\mathrm{sign}(\dot{y}_{\mathrm{p}}) , \tag{9}$$

where μ_{p} is the Coulomb friction coefficient and $\mathrm{sign}(x)$ is the function defined by

$$\mathrm{sign}(x) = \begin{cases} 1 & \text{if } x > 0 \\ 0 & \text{if } x = 0 \\ -1 & \text{if } x < 0 \end{cases} .$$

On the other hand, there is a torque over the $\boldsymbol{z}_{\mathrm{p}}^{\mathrm{h}}$ axis produced by the movement of the x_{h} coordinate and the change of the pressure distribution which in turn is induced by the acceleration on the θ coordinate [16], and is given by

$$\tau_\phi = -\mu_\phi I_{\mathrm{px}}\mathrm{sign}(\dot{x}_{\mathrm{p}})\ddot{\theta} , \tag{10}$$

where I_{px} is the $(1,1)$ component of the tensor $\boldsymbol{I}_{\mathrm{p}}$. By Newton's third law of motion, there must be a reaction torque acting on the θ coordinate. However, this torque can be neglected by assuming that the inertia of the plate is much bigger than that of the disk.

Overall, the non-conservative and external forces are represented by the vector

$$\boldsymbol{\xi} = \begin{bmatrix} f_{\mathrm{h}} & \tau_\theta & f_{\mathrm{x}} & f_{\mathrm{y}} & \tau_\phi \end{bmatrix}^{\mathrm{T}} , \tag{11}$$

where f_{h} is the external force applied over the plate in the $\boldsymbol{x}_{\mathrm{h}}$ direction and τ_θ is the external torque over the same axis.

A further simplification can be made if it is considered the linear and angular accelerations of the plate as inputs, *i.e.*

$$\boldsymbol{u} \triangleq \begin{bmatrix} u_{\mathrm{h}} & u_\theta \end{bmatrix}^{\mathrm{T}} \triangleq \begin{bmatrix} \ddot{x}_{\mathrm{h}} & \ddot{\theta} \end{bmatrix}^{\mathrm{T}} . \tag{12}$$

In order to employ continuous tools to analyze the system dynamics, we make the following approximation of the sign function

$$\mathrm{sign}(x_i) \approx \tanh(\alpha_i x_i) , \tag{13}$$

where each α_i is a positive constant.

Since we are interested in controlling the disk rotation speed, we define the error

$$\tilde{\dot{\phi}} = \dot{\phi} - \dot{\phi}_{\mathrm{d}} , \tag{14}$$

where $\dot{\phi}_{\mathrm{d}}$ is the desired disk rotation speed. Now, let the state space vector $\boldsymbol{x} \in \mathbb{R}^9$ be defined by

$$\begin{aligned} \boldsymbol{x} &= \begin{bmatrix} x_1 & x_2 & \cdots & x_9 \end{bmatrix}^{\mathrm{T}} \\ &\triangleq \begin{bmatrix} x_{\mathrm{h}} & \theta & x_{\mathrm{p}} & y_{\mathrm{p}} & \dot{x}_{\mathrm{h}} & \dot{\theta} & \dot{x}_{\mathrm{p}} & \dot{y}_{\mathrm{p}} & \tilde{\dot{\phi}} \end{bmatrix}^{\mathrm{T}} . \end{aligned} \tag{15}$$

[2]Due to the slight abuse of notation, care should be taken to not confuse the scalars x_{h}, x_{p}, and y_{p} with the vectors $\boldsymbol{x}_{\mathrm{h}}$, $\boldsymbol{x}_{\mathrm{p}}$, and $\boldsymbol{y}_{\mathrm{p}}$.

Then the system dynamics can be put in the form

$$\dot{\boldsymbol{x}} = \boldsymbol{f}(\boldsymbol{x}) + \boldsymbol{g}_1 u_{\mathrm{h}} + \boldsymbol{g}_2(\boldsymbol{x}) u_\theta \,, \tag{16}$$

where

$$\boldsymbol{f}(\boldsymbol{x}) = \begin{bmatrix} x_5 \\ x_6 \\ x_7 \\ x_8 \\ \boldsymbol{f}_2(\boldsymbol{x}) \end{bmatrix} \qquad \boldsymbol{g}_1 = \begin{bmatrix} \mathbf{0}_4 \\ \boldsymbol{g}_{12} \end{bmatrix} \qquad \boldsymbol{g}_2(\boldsymbol{x}) = \begin{bmatrix} \mathbf{0}_4 \\ \boldsymbol{g}_{22}(\boldsymbol{x}) \end{bmatrix} , \tag{17}$$

with

$$\boldsymbol{f}_2(\boldsymbol{x}) = \begin{bmatrix} 0 \\ 0 \\ -g\mu_{\mathrm{p}} \tanh(k_7 x_7) \\ -g\mu_{\mathrm{p}} \tanh(k_8 x_8) - g \sin(x_2) + x_4 x_6^2 \\ 0 \end{bmatrix} \tag{18}$$

$$\boldsymbol{g}_{12} = \begin{bmatrix} 1 & 0 & -1 & 0 & 0 \end{bmatrix}^{\mathrm{T}} \tag{19}$$

$$\boldsymbol{g}_{22}(\boldsymbol{x}) = \begin{bmatrix} 0 & 1 & 0 & 0 & -\mu_\phi \left(I_{\mathrm{px}} / I_{\mathrm{pz}} \right) \tanh(k_7 x_7) \end{bmatrix}^{\mathrm{T}} , \tag{20}$$

where I_{pz} is the $(3,3)$ component of the inertia tensor $\boldsymbol{I}_{\mathrm{p}}$.

For the present system, the *exact linearization via feedback* cannot be applied, since it does not satisfy the necessary condition (iii) of [18, Theorem 2.4, p. 250], that is, the distribution $G_0 \triangleq \operatorname{span}\{\boldsymbol{g}_1, \boldsymbol{g}_2\}$ fails to be involutive. Notice also that (16) has drift for which Chow's theorem does not apply. Therefore, a less strong property, *i.e. accessibility* will be investigated to gain some insight for the control design. By computing the Philip Hall basis [19, p. 344] with the vector fields $\boldsymbol{f}$, $\boldsymbol{g}_1$, and $\boldsymbol{g}_2$, one can check that the *accessibility distribution* is of dimension 9 in the set $\mathcal{D} = \left\{ \boldsymbol{x} \in \mathbb{R}^9 : \dot{\theta} \neq 0, \dot{x}_{\mathrm{p}} \neq 0, y_{\mathrm{p}} \neq 0 \right\}$, and thus the system is *accessible*. Furthermore, by computing the base

$$\{\boldsymbol{g}_1, \boldsymbol{g}_2, [\boldsymbol{g}_1, \boldsymbol{f}], [\boldsymbol{g}_2, \boldsymbol{f}], [\boldsymbol{g}_1, \boldsymbol{g}_2], [\boldsymbol{f}, [\boldsymbol{g}_1, \boldsymbol{f}]], [\boldsymbol{f}, [\boldsymbol{g}_2, \boldsymbol{f}]], [\boldsymbol{f}, [\boldsymbol{g}_1, \boldsymbol{g}_2]], [\boldsymbol{g}_1, [\boldsymbol{g}_1, \boldsymbol{f}]], [\boldsymbol{g}_2, [\boldsymbol{g}_2, \boldsymbol{f}]]\}$$

one can prove that the system is *strongly accessible* in $\mathcal{D}$ [20, p. 180]. However, if the centripetal force term $x_4 x_6^2$ is neglected, as is commonly assumed in the related literature (see for example [15], [16]), the strong accessibility condition is no longer met, but only the accessibility one, restricted to $\mathcal{D}_{\mathrm{a}} = \left\{ \boldsymbol{x} \in \mathbb{R}^9 : \dot{x}_{\mathrm{p}} \neq 0, \dot{y}_{\mathrm{p}} \neq 0 \right\}$. The following assumption is addressed in this work.

Assumption 1: The centrifugal force term $x_4 x_6^2$ in (16) can be neglected. □

Remark 1: This assumption is made to simplify the controller design and the stability analysis, but the term $x_4 x_6^2$ is kept for simulating the system dynamics. □

III. Control Design and Stability Analysis

The control objective of this work is inducing a rotating movement on the disk dough at a desired angular speed $\dot{\phi}_{\mathrm{d}}$ while keeping the remaining coordinates as close to zero as possible.

A. Control design

For fulfill the objective mentioned above, we propose the following control law

$$u_{\mathrm{h}} = -k_1 x_1 - k_5 x_5 + a_{\mathrm{h}} \sin(\omega_{\mathrm{h}} t) \tag{21}$$

$$u_\theta = \frac{\tanh(k_7 x_7) I_{\mathrm{pz}}}{\mu_\phi I_{\mathrm{px}}} k_9 x_9 - k_2 x_2 - k_6 x_6 \,. \tag{22}$$

The first term of (21) is a PD control to stabilize the peel linear direction plus a feedforward term, $a_{\mathrm{h}} \sin(\omega_{\mathrm{h}} t)$, to ensure the condition $\dot{x}_{\mathrm{p}} = x_7 \neq 0$. On the other hand, the control law (22) is a PD control to stabilize the peel orientation plus a nonlinear term to induce a rotation in the disk by exploiting the torque generated in (10).

The corresponding closed-loop dynamics is given by

$$\begin{aligned}
\dot{x}_1 =& x_5 \,, \quad \dot{x}_2 = x_6 \,, \quad \dot{x}_2 = x_7 \,, \quad \dot{x}_4 = x_8, \\
\dot{x}_5 =& -k_1 x_1 - k_5 x_5 + a_{\mathrm{h}} \sin(\omega_{\mathrm{h}} t) \\
\dot{x}_6 =& -k_2 x_2 - k_6 x_6 + \frac{I_{\mathrm{pz}}}{\mu_\phi I_{\mathrm{px}}} \tanh(k_7 x_7) k_9 x_9 \\
\dot{x}_7 =& -g\mu_{\mathrm{p}} \tanh(k_7 x_7) + k_1 x_1 + k_5 x_5 - a_{\mathrm{h}} \sin(\omega_{\mathrm{h}} t) \\
\dot{x}_8 =& -g\mu_{\mathrm{p}} \tanh(k_8 x_8) - g \sin(x_2) \\
\dot{x}_9 =& -k_9 x_9 \tanh^2(k_7 x_7) \\
& + \frac{\mu_\phi I_{\mathrm{px}}}{I_{\mathrm{pz}}} \tanh(k_7 x_7) \left(k_2 x_2 + k_6 x_6 \right) \,.
\end{aligned} \tag{23}$$

B. Stability analysis

The following analysis will be carried out considering that stationary state has reached. Furthermore, the closed-loop dynamics is divided into the four subsystems shown in Figure 2.

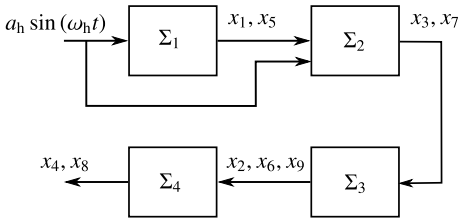

Fig. 2. Closed-loop dynamics.

1) The first subsystem Σ_1, comprised of the states x_1 and x_5, is a linear stable system with poles arbitrarily chosen by means of the gains k_1 and k_5, under the effect of the sinusoidal input $a_{\mathrm{h}} \sin(\omega_{\mathrm{h}} t)$. In stationary state the amplitude of the states x_1 and x_5 are sinusoidals with frequency ω_{h} and amplitude easily calculated to be

$$|x_1| = a_{\mathrm{h}} / D(k_1, k_5, \omega_{\mathrm{h}}) \tag{24}$$

$$|x_5| = a_{\mathrm{h}} \omega_{\mathrm{h}} / D(k_1, k_5, \omega_{\mathrm{h}}) \,, \tag{25}$$

where

$$D(k_1, k_5, \omega_{\mathrm{h}}) = \sqrt{\left(k_1 - \omega_{\mathrm{h}}^2\right)^2 + k_5^2 \omega_{\mathrm{h}}^2} \,. \tag{26}$$

2) The second subsystem, corresponding to the states x_3 and x_7, will be analyzed by employing the *describing*

function method [21, p. 157], for which the configuration shown in Figure 3 is considered with input $u = -u_{\rm h}$ and output $y = x_7$. The describing function

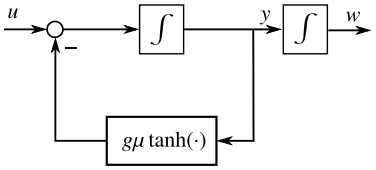

Fig. 3. Nonlinear feedback loop.

that approximates the nonlinearity in the Σ_2 subsystem for $\alpha_7 >> 0$ in (13), is given by

$$g\mu_{\rm p}\tanh(\cdot) \approx \frac{4g\mu_{\rm p}}{\pi A(\cdot)}\,, \tag{27}$$

where $A(\cdot)$ is the input amplitude of the nonlinear block signal, which is assumed to be sinusoidal. The approximate closed-loop transfer function of the subsystem Σ_2 is

$$y(s) = \left(\frac{1}{s + 4g\mu_{\rm p}/(\pi A(\cdot))}\right) u(s) = h(s)u(s)\,, \tag{28}$$

where s is a complex variable of Laplace domain. According to [22, Ch. 3] the output of this system is the sum of a self-oscillatory response and a forced response. The frequency of the self oscillatory component $\omega_{\rm s}$ is obtained by solving the equation

$$j\omega_{\rm s} = 4g\mu_{\rm p}/(\pi A(\cdot))\,. \tag{29}$$

Since $A(\cdot)$ is a positive and real function, no unforced periodic response is present. On the other hand, the gain for the closed-loop pseudo-transfer function can be computed as

$$|h(s)| = \frac{1}{\sqrt{\omega_{\rm h}^2 + 16g^2\mu_{\rm p}^2/(\pi^2 A^2(\cdot))}}\,, \tag{30}$$

which is minimum at zero for $A(\cdot) \to 0$ and maximum at $1/\omega_{\rm h}$ for $A(\cdot) \to \infty$. The input to this subsystem is $u = -u_{\rm h}$, which is a sinusoidal signal with zero mean, frequency $\omega_{\rm h}$ and amplitude bounded by

$$|u_{\rm h}| \le a_{\rm h}\left(\frac{k_1 + k_5\omega_{\rm h}}{D(k_1, k_5, \omega_{\rm h})} + 1\right)\,. \tag{31}$$

Thus, the approximate steady state output of this subsystem is a sinusoidal with zero mean given by

$$x_7 = a_7 \sin\left(\omega_{\rm h} t + \phi_7\right)\,, \tag{32}$$

where

$$|a_7| \le \frac{a_{\rm h}}{\omega_{\rm h}}\left(\frac{k_1 + k_5\omega_{\rm h}}{D(k_1, k_5, \omega_{\rm h})} + 1\right) \tag{33}$$

and ϕ_7 is the phase shift given by

$$\phi_7 = \mathrm{atan2}(-a_{\rm h}\omega_{\rm h}, 4g\mu_{\rm p}/(\pi A(\cdot)))\,, \tag{34}$$

which can be bounded by $-\pi/2 \le \phi_7 \le 0$. The steady state response for x_3 can be approximated by

$$x_3 = a_3 \sin\left(\omega_{\rm h} t + \phi_3\right) + c_3\,, \tag{35}$$

where ϕ_3 is a phase shift, c_3 is a bias constant, and

$$|a_3| \le \frac{a_{\rm h}}{\omega_{\rm h}^2}\left(\frac{k_1 + k_5\omega_{\rm h}}{D(k_1, k_5, \omega_{\rm h})} + 1\right)\,. \tag{36}$$

3) To show stability of this subsystem we first recall the following [23, Theorem 10.3].
Theorem 1: Consider the system

$$\dot{\boldsymbol{x}} = \boldsymbol{f}(\boldsymbol{x}) + \epsilon\boldsymbol{g}(t, \boldsymbol{x}, \epsilon)\,. \tag{37}$$

Suppose

- $\boldsymbol{f}$, $\boldsymbol{g}$, and their first partial derivatives with respect to $\boldsymbol{x}$ are continuous and bounded for all $(t, \boldsymbol{x}, \epsilon) \in [0, \infty) \times D_0 \times [-\epsilon_0, \epsilon_0]$, for every compact set $D_0 \subset D$, where $D \subset \mathbb{R}^n$ is a domain that contains the origin;
- The origin is an exponentially stable equilibrium point of the autonomous system

$$\dot{\boldsymbol{x}} = \boldsymbol{f}(\boldsymbol{x})\,; \tag{38}$$

- $\boldsymbol{g}(t, \boldsymbol{x}, \epsilon)$ is T-periodic in t.

Then, there exist positive constants ϵ^* and k such that for all $|\epsilon| < \epsilon^*$, equation (37) has a unique T-periodic solution $\bar{\boldsymbol{x}}(t, \epsilon)$ with the property that $\|\bar{\boldsymbol{x}}(t, \epsilon)\| \le k|\epsilon|$. Moreover, this solution is exponentially stable. □
By employing the identity $\tanh^2(x) = 1 - \mathrm{sech}^2(x)$, the dynamics of the subsystem Σ_3 can be written as equation (37) with $\boldsymbol{x} = \begin{bmatrix} x_2 & x_6 & x_9 \end{bmatrix}^{\rm T}$ and

$$\boldsymbol{f} = \begin{bmatrix} x_6 \\ -k_2 x_2 - k_6 x_6 \\ -k_9 x_9 \end{bmatrix} \tag{39}$$

$$\boldsymbol{g} = \begin{bmatrix} 0 \\ \frac{1}{c_\mu}\tanh(k_7 x_7) k_9 x_9 \\ g_3(\boldsymbol{x}) \end{bmatrix}\,, \tag{40}$$

where

$$\begin{aligned} g_3(\boldsymbol{x}) = \; & \mathrm{sech}^2(k_7 x_7) k_9 x_9 \\ & + c_\mu \tanh(k_7 x_7)\left(k_2 x_2 + k_6 x_6\right)\,, \end{aligned}$$

$c_\mu = \mu_\phi I_{\rm px}/I_{\rm pz}$, $\boldsymbol{f}(\boldsymbol{x}) = \boldsymbol{f}$ and $\boldsymbol{g}(t, \boldsymbol{x}, \epsilon) = \boldsymbol{g}$, with $\epsilon = 1$. As proven before, the steady state solution for x_7 is a T-periodic function of time t, with period $T = 2\pi/\omega_{\rm h}$, and so it is $\boldsymbol{g}$ in (40). It is easy to show that the autonomous subsystem $\dot{\boldsymbol{x}} = \boldsymbol{f}(\boldsymbol{x})$, with $\boldsymbol{f}(\boldsymbol{x})$ defined in (39), is exponentially stable. By applying Theorem 1 in the region $\mathbb{D} \triangleq \{\boldsymbol{x} : \|\boldsymbol{x}\| \le \rho\}$, with $\rho > 0$, one can conclude that the solution trajectories for the states $\boldsymbol{x} = \begin{bmatrix} x_2 & x_6 & x_9 \end{bmatrix}^{\rm T}$ are T-periodic functions of time, and the states converge exponentially to these solutions. As stated in Theorem 1, the periodic solution is bounded by $\|\bar{\boldsymbol{x}}(t, \epsilon)\| \le k|\epsilon|$. Furthermore, from the theory of linear bounded input–bounded output systems,

TABLE I

PARAMETERS USED FOR SIMULATION.

Meaning	Parameter	Value
Pizza mass	m_{p}	$0.25\,\mathrm{kg}$
Pizza x-inertia moment	I_{px}	$0.01\,\mathrm{kg\,m^2}$
Pizza z-inertia moment	I_{pz}	$0.028\,\mathrm{kg\,m^2}$
Linear Coulomb friction coefficient	μ_{p}	0.5
Rotational Coulomb friction coefficient	μ_{ϕ}	0.5
Gravity acceleration constant	g	$9.81\,\mathrm{m/s^2}$

the ultimate bound $k|\epsilon|$ can be made arbitrarily small by making the gains k_2, k_6, and k_9 arbitrarily large.

4) For this subsystem consider again the block diagram depicted in Figure 3, with $u = -g\sin(x_2)$, $y = x_8$, and $w = x_4$. The approximate transfer function is given by (28). By the same arguments given in point 2, the solution trajectories for this system can be approximated by

$$x_4 = a_4 \sin(\omega_{\mathrm{h}} t + \phi_4) + c_4 \tag{41}$$

$$x_8 = a_8 \sin(\omega_{\mathrm{h}} t + \phi_8)\,, \tag{42}$$

where c_4 is a bias constant and

$$a_4 \leq c_8 g/\omega_{\mathrm{h}}^2\,, \quad a_8 \leq c_8 g/\omega_{\mathrm{h}}\,, \tag{43}$$

with $c_8 = \sup_t(|\sin(x_2(t))|)$.

Overall, we have shown that the approximate solutions of the closed-loop system are bounded and periodic. Moreover, the ultimate bound for the states x_2, x_6, and x_9 can be driven arbitrarily close to zero, which means that the peel will be as close as desired to the horizontal position and that the pizza rotation speed will be arbitrarily close to the desired value, *i.e.* $\dot{\phi} \approx \dot{\phi}_d$.

IV. NUMERICAL SIMULATION

To validate the results of Section III, a numerical simulation is proposed. As mentioned before, we have kept the centrifugal term $x_4 x_6^2$ in (20) to test the robustness of the control design. The parameters considered for the system are given in Table I. The controller parameters in (21)–(22) were chosen empirically as $\omega_{\mathrm{h}} = 18\,\mathrm{rad/s}$, $a_{\mathrm{h}} = 2$, $k_1 = 10$, $k_2 = 10$, $k_5 = 10$, $k_6 = 50$, $k_7 = 20$, and $k_9 = 40$. The sample time considered for the control loop was $T = 5\,\mathrm{ms}$. The desired velocity for the disk rotation is $\dot{\phi}_{\mathrm{d}} = 1\,\mathrm{rad/s}$ in counterclockwise direction. The desired rotation speed is shown in Figure 4 along with the actual speed. In this figure, it can be appreciated that the disk rotation speed is very close to the desired one in steady state. In Figure 5, the phase portrait of x_{h} is shown. In this plot, and in all following plots, a blue marker is used to indicate the initial point, a green line to denote the first 15 seconds (transient response) and a red line to indicate the last 15 seconds (steady state). In this figure it can be appreciated that the x_{h} and $\dot{x}_{\mathrm{h}}$ coordinates keep oscillating around zero. The amplitude of x_{h} coincides with the one predicted by (24), *i.e* $|x_h| = 0.0055\,\mathrm{m}$. On the other hand, the phase portrait for the θ coordinate is shown in Figure 6. In this figure, it can be seen that this coordinate remains oscillating very close to zero in stationary state. This in accordance with the stability analysis of Section III. In Figure 7, the phase portrait for the x_{p} coordinate is shown. The theoretical bounds for the amplitude of the oscillations of $x_3 = x_{\mathrm{p}}$ computed in (36) and $x_7 = \dot{x}_{\mathrm{p}}$ in (33) are $|a_3| \leq 0.0094\,\mathrm{m}$ and $|a_7| \leq 0.1694\,\mathrm{m/s}$, respectively, which are very conservative ones, as can be seen in the figure. The reason behind these large margins, is simply because we are taking the worst case for the pseudo-transfer function gain in (30). Finally, the phase portrait for the y_{p} coordinate is displayed in Figure 8. As can be seen in this figure, the oscillation amplitude of this coordinate can be made arbitrarily small, as it depends on the amplitude of θ, which in turn can be made arbitrarily small. However, in this case there is a non-negligible bias term of about $6\,\mathrm{mm}$ as stated in (41).

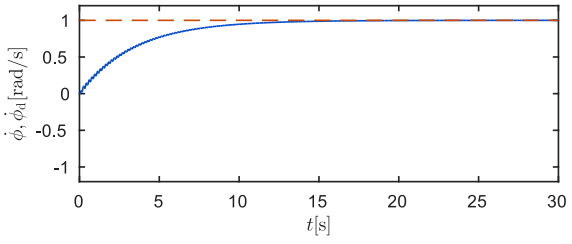

Fig. 4. Pizza rotation speed: real (—), desired (- - -)

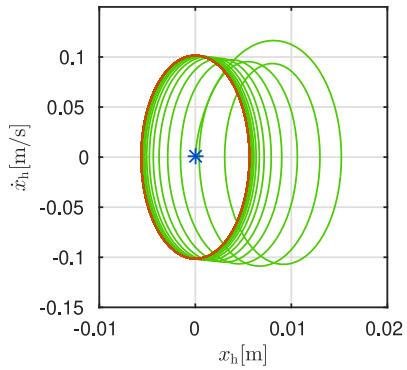

Fig. 5. Phase portrait of x_{h}: $t = 0\,\mathrm{s}$ (∗), $t \leq 15\,\mathrm{s}$ (—), $t > 15\,\mathrm{s}$ (—).

V. CONCLUSIONS

A closed-loop control strategy for an underactuated non-prehensile manipulation system was proposed. The control strategy is based on the properties of the dynamical model of the system plus PD controllers. The controllability of this model was studied to understand the intrinsic limitations of the system. Then, a closed loop stability analysis was carried out, assuming a steady state. This analysis showed that all the states are bounded and that some of them could be delivered close to zero arbitrarily. It also predicted the oscillatory response of some states and the amplitude of these oscillations, which was then verified in the numerical simulation. As a future work, it will be studied the possibility

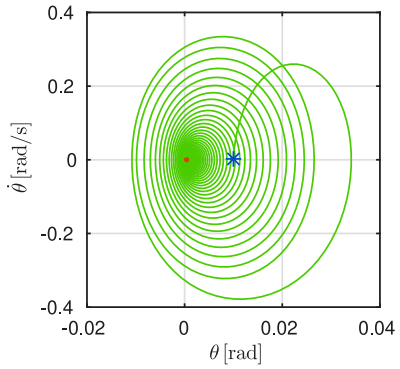

Fig. 6. Phase portrait of θ: $t = 0\,\mathrm{s}$ (∗), $t \leq 15\,\mathrm{s}$ (—), $t > 15\,\mathrm{s}$ (—).

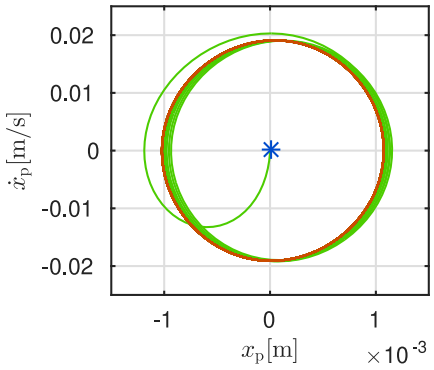

Fig. 7. Phase portrait of x_p: $t = 0\,\mathrm{s}$ (∗), $t \leq 15\,\mathrm{s}$ (—), $t > 15\,\mathrm{s}$ (—).

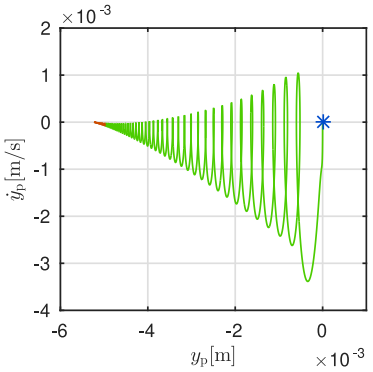

Fig. 8. Phase portrait of y_p: $t = 0\,\mathrm{s}$ (∗), $t \leq 15\,\mathrm{s}$ (—), $t > 15\,\mathrm{s}$ (—).

to practically stabilize all the states (drive all of them close to zero, without bias). This could be done either by re-designing the controller or by adding degrees of freedom in the manipulating system. It also remains to carry out experiments in a real mechanical system. One of the main practical limitations is the required measurement, which is to be acquired using a vision system. The low sampling time, along with the noise and the quantization phenomena, is some of the main inherent problems to this kind of sensors in such a particular application.

REFERENCES

[1] K. M. Lynch and M. T. Mason, "Dynamic nonprehensile manipulation: Controllability, planning, and experiments," *The International Journal of Robotics Research*, vol. 18, no. 1, pp. 64–92, 1999.

[2] F. Ruggiero, V. Lippiello, and B. Siciliano, "Nonprehensile dynamic manipulation: A survey," *IEEE Robotics and Automation Letters*, vol. 3, no. 3, pp. 1711–1718, 2018.

[3] K. M. Lynch, N. Shiroma, H. Arai, and K. Tanie, "The roles of shape and motion in dynamic manipulation: The butterfly example," in *IEEE International Conference on Robotics and Automation (ICRA). Proceedings. 1998*, vol. 3. IEEE, 1998, pp. 1958–1963.

[4] A. Donaire, F. Ruggiero, L. R. Buonocore, V. Lippiello, and B. Siciliano, "Passivity-based control for a rolling-balancing system: The nonprehensile disk-on-disk," *IEEE Transactions on Control System Technology*, vol. 25, no. 6, pp. 2135–2142, 2017.

[5] A. Gutiérrez-Giles, F. Ruggiero, V. Lippiello, and B. Siciliano, "Nonprehensile manipulation of an underactuated mechanical system with second-order nonholonomic constraints: The robotic hula-hoop," *IEEE Robotics and Automation Letters*, vol. 3, no. 2, pp. 1136–1143, 2018.

[6] M. Higashimori, Y. Omoto, and M. Kaneko, "Non-grasp manipulation of deformable object by using pizza handling mechanism," in *IEEE International Conference on Robotics and Automation (ICRA)*. IEEE, 2009, pp. 120–125.

[7] P. Lertkultanon and Q.-C. Pham, "Dynamic non-prehensile object transportation," in *2014 13th International Conference on Control Automation Robotics & Vision (ICARCV)*. IEEE, 2014, pp. 1392–1397.

[8] A. C. Satici, F. Ruggiero, V. Lippiello, and B. Siciliano, "A coordinate-free framework for robotic pizza tossing and catching," in *IEEE International Conference on Robotics and Automation (ICRA)*. IEEE, 2016, pp. 3932–3939.

[9] T. Tsuji, K. Kutsuzawa, and S. Sakaino, "Optimized trajectory generation based on model predictive control for turning over pancakes," *IEEJ Journal of Industry Applications*, vol. 7, no. 1, pp. 22–28, 2018.

[10] P. Cigliano, V. Lippiello, F. Ruggiero, and B. Siciliano, "Robotic ball catching with an eye-in-hand single-camera system," *IEEE Transactions on Control Systems Technology*, vol. 23, no. 5, pp. 1657–1671, 2015.

[11] F. Ruggiero, A. Petit, D. Serra, A. C. Satici, J. Cacace, A. Donaire, F. Ficuciello, L. R. Buonocore, G. A. Fontanelli, V. Lippiello *et al.*, "Nonprehensile manipulation of deformable objects: Achievements and perspectives from the rodyman project," *IEEE Robotics & Automation Magazine*, 2018.

[12] M. Higashimori, K. Utsumi, and M. Kaneko, "Dexterous hyper plate inspired by pizza manipulation," in *IEEE International Conference on Robotics and Automation (ICRA)*. IEEE, 2008, pp. 399–406.

[13] D. S. Reznik and J. F. Canny, "C'mon part, do the local motion!" in *IEEE International Conference on Robotics and Automation (ICRA)*, vol. 3. IEEE, 2001, pp. 2235–2242.

[14] T. H. Vose, P. Umbanhowar, and K. M. Lynch, "Friction-induced lines of attraction and repulsion for parts sliding on an oscillated plate," *IEEE Transactions on Automation Science and Engineering*, vol. 6, no. 4, pp. 685–699, 2009.

[15] T. H. Vose, P. Umbanhowar, and K. M. Lynch, "Sliding manipulation of rigid bodies on a controlled 6-dof plate," *The International Journal of Robotics Research*, vol. 31, no. 7, pp. 819–838, 2012.

[16] M. Higashimori, K. Utsumi, Y. Omoto, and M. Kaneko, "Dynamic manipulation inspired by the handling of a pizza peel," *IEEE Transactions on Robotics*, vol. 25, no. 4, pp. 829–838, 2009.

[17] B. Siciliano, L. Sciavicco, L. Villani, and G. Oriolo, *Robotics: modelling, planning and control*. Springer Science & Business Media, 2010.

[18] A. Isidori, *Nonlinear Control Systems: An Introduction*. Springer-Verlag.

[19] R. M. Murray, Z. Li, S. S. Sastry, and S. S. Sastry, *A mathematical introduction to robotic manipulation*. CRC press, 1994.

[20] A. Bloch, J. Baillieul, P. Crouch, J. E. Marsden, D. Zenkov, P. S. Krishnaprasad, and R. M. Murray, *Nonholonomic mechanics and control*. Springer, 2003, vol. 24.

[21] J.-J. Slotine and W. Li, *Applied nonlinear control*. Prentice Hall Englewood Cliffs, NJ, 1991, vol. 199, no. 1.

[22] I. Boiko, *Discontinuous control systems: frequency-domain analysis and design*. Springer Science & Business Media, 2008.

[23] H. Khalil, *Nonlinear systems*, 3rd ed. Prentice-Hall, Englewood Cliffs, NJ, 2002.